High-pressure ultrasonic study of the commensurate-incommensurate spin-density-wave transition in an antiferromagnetic Cr-0.3 at. % Ru alloy single crystal

M. Cankurtaran,* G. A. Saunders, Q. Wang, and P. J. Ford
School of Physics, University of Bath, Claverton Down, Bath BA2 7AY, United Kingdom

H. L. Alberts
Department of Physics, Rand Afrikaans University, P.O. Box 524, Johannesburg 2000, South Africa
(Received 27 July 1992)

A comprehensive experimental study has been made of the elastic and nonlinear acoustic behavior of a dilute Cr alloy as it undergoes a commensurate (C)-incommensurate (I) spin-density-wave transition. Simultaneous measurements of the temperature dependence of ultrasonic wave velocity and attenuation of longitudinal and shear 10-MHz ultrasonic waves propagated along both the [100] and the [110] direction of Cr-0.3 at. % Ru alloy single crystal have been made in the temperature range 200–300 K. The temperature dependence of ultrasonic attenuation for each mode is characterized by a spikelike peak centered at T_{CI} (=238.6 K) (on cooling) and at T_{IC} (=255.6 K) (on warming). The velocities of both longitudinal and shear ultrasonic waves exhibit a large and steep increase at T_{CI} on cooling and a similar drop at T_{IC} on warming with a pronounced hysteresis between T_{IC} and T_{CI}. These observations show that the transition between the commensurate and incommensurate phases is first order. Measurements of the effects of hydrostatic pressure (up to 0.15 GPa) on the velocities of ultrasonic waves, which were made at several fixed temperatures between 248 and 297 K, show similar features: a steep increase at P_{CI} (increasing pressure) and a similar drop at P_{IC} (decreasing pressure) with a well-defined hysteresis. Both T_{CI} and T_{IC} increase strongly and approximately linearly with pressure, the mean values of dT_{CI}/dP and dT_{IC}/dP being (333±3) K/GPa and (277±5) K/GPa, respectively. The pressure and temperature dependencies of the anomalies in the ultrasonic wave velocity have been used to locate both the C-I and I-C boundaries on the magnetic P-T phase diagram. There is a triple point (at about 315 K and 0.22 GPa) where the paramagnetic, commensurate, and incommensurate spin-density-wave phases coexist. Results for the complete sets of the elastic stiffness tensor components and their hydrostatic pressure derivatives have been used to evaluate the acoustic-mode Grüneisen parameters in both the commensurate and incommensurate phases. These quantify the vibrational anharmonicity of each acoustic phonon mode in the long-wavelength limit and establish which acoustic modes interact strongly with the spin-density waves. Pronounced longitudinal acoustic-mode softening under pressure results in negative Grüneisen parameters, a particularly marked feature of the commensurate phase.

I. INTRODUCTION

Below the Néel temperature T_N (=312 K) chromium has an antiferromagnetic structure with spin polarization described by a spin-density wave (SDW).[1–3] The wave vector $Q=(2\pi/a)(1-\delta)$ of the spin-density wave is incommensurate with the lattice spacing a. The incommensurability parameter δ is about 5% (Refs. 2 and 4–6) and is related to the difference in size of the electron and hole Fermi surface sheets centered, respectively, at Γ and H points of the Brillouin zone. Since the electron Fermi surface is slightly smaller than that containing holes, the nesting between the two Fermi surface sheets, which stabilizes the SDW,[7–9] can be improved by dilute alloying to increase the electron to atom (e/a) ratio. Neutron diffraction experiments have established that alloying of Cr with small amounts of metallic atoms (such as Mn, Ru, and Os) with more outer electrons raises the Fermi level, thereby increasing the size of the electron Fermi surface while at the same time decreasing that of the holes. This causes Q to increase. For an e/a ratio only slightly larger than the value of six for Cr, the antiferromagnetic SDW periodicity jumps from an incommensurate (I) to a commensurate (C) state.[4,10] Application of hydrostatic pressure can also introduce a change in the electronic structure (and hence in the SDW characteristics) of Cr and its dilute alloys.

The magnetic phase diagram of many dilute Cr alloys exhibits a triple point where the paramagnetic, the commensurate-SDW (CSDW) and the incommensurate-SDW (ISDW) phases coexist.[11] The CSDW to paramagnetic or the ISDW to paramagnetic transitions at the Néel temperature of these alloys are usually characterized by large anomalies in the temperature dependence of their physical properties. The anomalies at T_N, and their concentration and pressure dependences, have been extensively studied in several dilute Cr alloys through electrical resistivity, magnetic susceptibility, thermal expansion, and neutron diffraction measurements.[12] However, studies of the behavior of physical properties with pressure in the vicinity of the incommensurate-commensurate transition temperature (T_{IC}) are less extensive than those at T_N, since the electron transport properties, such as the electrical resistivity, usually show either no effect or only

small effects at T_{IC}.

Several experimental studies have been made of the elastic stiffness moduli of Cr and dilute Cr alloys and their behavior with temperature.[13–22] Recently, it has been found[19,22] that the elastic stiffness of dilute Cr-Ru alloys show well-defined anomalies at T_{IC}. This is the only Cr alloy system known for which all the single-crystal elastic stiffnesses show marked anomalies near T_{IC}. Thus ultrasonic wave velocity measurements can provide a sensitive tool for studying the ISDW to CSDW transition. However, with the exception of an initial study on the longitudinal modes only,[21] there has been no work on the effects of hydrostatic pressure on the elastic and an elastic behavior in the vicinity of any *I-C* SDW transition. The preliminary work on Cr-0.3 at. % Ru indicated that there is a strong magnetoelastic interaction leading to softening of the long-wavelength longitudinal acoustic phonons under pressure, which had not been previously recognized. Although the data[21] for the pressure dependence of the longitudinal-mode ultrasonic wave velocities relate directly to the pressure dependence of the elastic stiffness, the actual values of the pressure derivatives $(\partial C_{IJ}/\partial P)$ of the elastic tensor components C_{IJ} could not be extracted because a complete set of data was not obtained. A complete study of each of the stiffness tensor components is essential for understanding, and developing, a fundamental microscopic theory of the magnetoelasticity of SDW systems which is still lacking.

Ruthenium is a nonmagnetic element and should not introduce local magnetic moments in the Cr host. The magnetic phase diagrams of dilute Cr-Ru alloys containing 0.3 and 0.6 at. % Ru exhibit three antiferromagnetic phases:[23,24] (i) at low temperatures, a longitudinal incommensurate phase existing up to the spin-flip temperature T_{SF}, (ii) above T_{SF}, a transverse incommensurate phase up to T_{IC} (the incommensurate to commensurate transition temperature), (iii) above T_{IC} and below T_N, a magnetic structure commensurate with the lattice for which the SDW wave vector Q is equal to $2\pi/a$. For a Cr alloy containing nominally 0.3 at. % Ru, the following transition temperatures at atmospheric pressure have been measured on the warming cycle: T_{SF}, 114 (Ref. 24) and 87 K;[22] T_{IC}, about 250 K [which was observed to be broad, ranging from 240 to 270 K (Ref. 24)] and 257 K;[22] T_N, 377,[23] 380,[24] and 402 K.[22] For concentrations in the range between about 1 and 5 at. % Ru the commensurate phase only has been found between 4 K and the Néel temperature.[24]

The aim of the present work has been to measure all the elastic stiffness tensor components as a function of temperature and hydrostatic pressure in an antiferromagnetic Cr-0.3 at. % Ru alloy single crystal in both the commensurate and incommensurate phases as well as through the CSDW-ISDW transition. This concentration is ideally suited for such a study as the CSDW-ISDW transition at atmospheric pressure occurs at about 250 K, which is readily accessible to high-pressure ultrasonic experiments. Measurements of the elastic stiffness tensor components and their hydrostatic pressure derivatives quantify the acoustic-mode vibrational anharmonicity, through the mode Grüneisen parameters. This information is necessary for an understanding of the acoustic-phonon interaction with the SDW and addresses the question of whether the strong magnetoelastic coupling at the CSDW-ISDW transition takes place solely with the volume strain or if there are also contributions from shear strain.[25,12] In addition, any theoretical study of the magnetovolume and magnetoelastic effects requires data on the bulk modulus and its hydrostatic pressure derivative; these have been obtained with precision over a wide range of temperature from the present high-pressure ultrasonic experiments. Another outcome relevant to the theoretical understanding of the CSDW-ISDW transition in these alloys is an accurate determination of the pressure dependence dT_{CI}/dP of the transition temperature and hence the corresponding magnetic Grüneisen parameter.[12] The results have also been used to map the boundary between the CSDW and ISDW phases in the *P-T* phase diagram.

II. EXPERIMENTAL PROCEDURES

The Cr-0.3 at. % Ru single crystal is the same as that used by Alberts *et al.*[21] It was grown from high-purity elements by a floating-zone technique using rf heating. Electron microprobe analysis showed that it was reasonably homogeneous with an actual composition of (0.28 ± 0.02) at. % Ru. The crystal was oriented to $\pm0.5°$ using Laue back-reflection photography. An ultrasonic sample was cut and polished, using a spark cutter, having two pairs of parallel faces, normal to the required propagation directions along the [100] and [110] crystallographic axes.

Ultrasonic wave velocity and attenuation measurements were made along the [100] and [110] directions. 10-MHz ultrasonic pulses were generated and detected by *X*- and *Y*-cut quartz transducers bonded to the sample using Nonaq for low-temperature experiments or Dow resin for high-pressure experiments. Ultrasonic pulse transit times were measured using the pulse-echo overlap technique[26] which is capable of resolving velocity changes of 1 part in 10^5 and is particularly well suited to determination of pressure- or temperature-induced changes in velocity. A correction was applied to the ultrasonic wave velocity for multiple reflections at the sample-transducer interface.[27] The measurements of the temperature dependences of ultrasonic wave velocity and attenuation were performed simultaneously in a closed cycle refrigerator in the temperature range 200–300 K. The temperature was changed at a rate of about 0.2 K min^{-1} during both cooling and warming cycles. In the transition region the temperature was altered in steps of 0.1 K and controlled to ±0.02 K. The attenuation measurements were made by matching a calibrated exponential curve to the ultrasonic pulse-echo train. The dependence of ultrasonic wave velocity on hydrostatic pressure was measured at several fixed temperatures between 248 and 297 K. Hydrostatic pressure up to about 0.15 GPa was applied using a piston and cylinder apparatus sealed with Teflon and Viton O rings. Silicone fluid was used as the pressure transmitting medium. The pressure was measured using the change in

resistance of a precalibrated manganin wire coil (fixed on the sample holder) inside the cell. Temperatures below room temperature were reached by cooling the pressure cell using alcohol, which is precooled with liquid nitrogen, circulating in a coil wrapped around the outside of the pressure cylinder. During pressure runs it was essential to ensure that velocity measurements were made at the same controlled temperature to within 0.2 K.

III. EXPERIMENTAL RESULTS FOR THE TEMPERATURE DEPENDENCES OF THE ELASTIC STIFFNESS TENSOR COMPONENTS, BULK MODULUS AND ULTRASONIC ATTENUATION

The temperature dependences of the three independent adiabatic elastic stiffness tensor components C_{11}, C_{44}, and $C'[=(C_{11}-C_{12})/2]$ and the bulk modulus B^S $(=C_{11}-4C'/3)$, determined at zero pressure from the ultrasonic velocity data and sample density $(=7160\ \mathrm{kg\,m^{-3}})$, are shown in Fig. 1. The effects of thermal expansion[19] on these elastic moduli have been estimated and found to be negligible, being within the experimental error. The results obtained during both cooling and warming cycles are shown. In the commensurate phase, on cooling from 300 K down to about 245 K, C_{11} [Fig. 1(a)] and B^S [Fig. 1(d)] increase; in contrast, the shear stiffness moduli C_{44} [Fig. 1(b)] and C' [Fig. 1(c)] decrease. On further cooling all the elastic moduli show a sharp increase centered at the same temperature (=238.6 K), which corresponds to the commensurate to incommensurate transition temperature T_{CI}.[22] In the incommensurate phase, below about 235 K, all the elastic moduli stiffen in the usual way as the temperature is decreased (Fig. 1). The relative increases incurred at T_{CI} in C_{11}, C_{44}, C', and B^S with respect to the bottom of the step are 6.1%, 2.1%, 4.4%, and 8.2%, respectively: although the magnetoelastic coupling is significantly stronger for the volume-dependent longitudinal modes, it also affects the shear modes. The data obtained in the warming cycle show a smooth decrease with temperature followed by a sharp drop centered at 255.6 K, which corresponds to the incommensurate to commensurate transition temperature T_{IC}. There is a pronounced hysteresis between about 235 and 257 K; the width $\Delta T(=T_{IC}-T_{CI})$ of the hysteresis is the same for all modes. Above about 257 K the elastic moduli show no thermal hysteresis between cooling and warming. When the temperature returns to 300 K the sound velocity and attenuation (see below) are restored to their initial values: the sample recovers back to its initial thermodynamic condition. In the incommensurate phase there is some hysteresis probably due to the domain wall

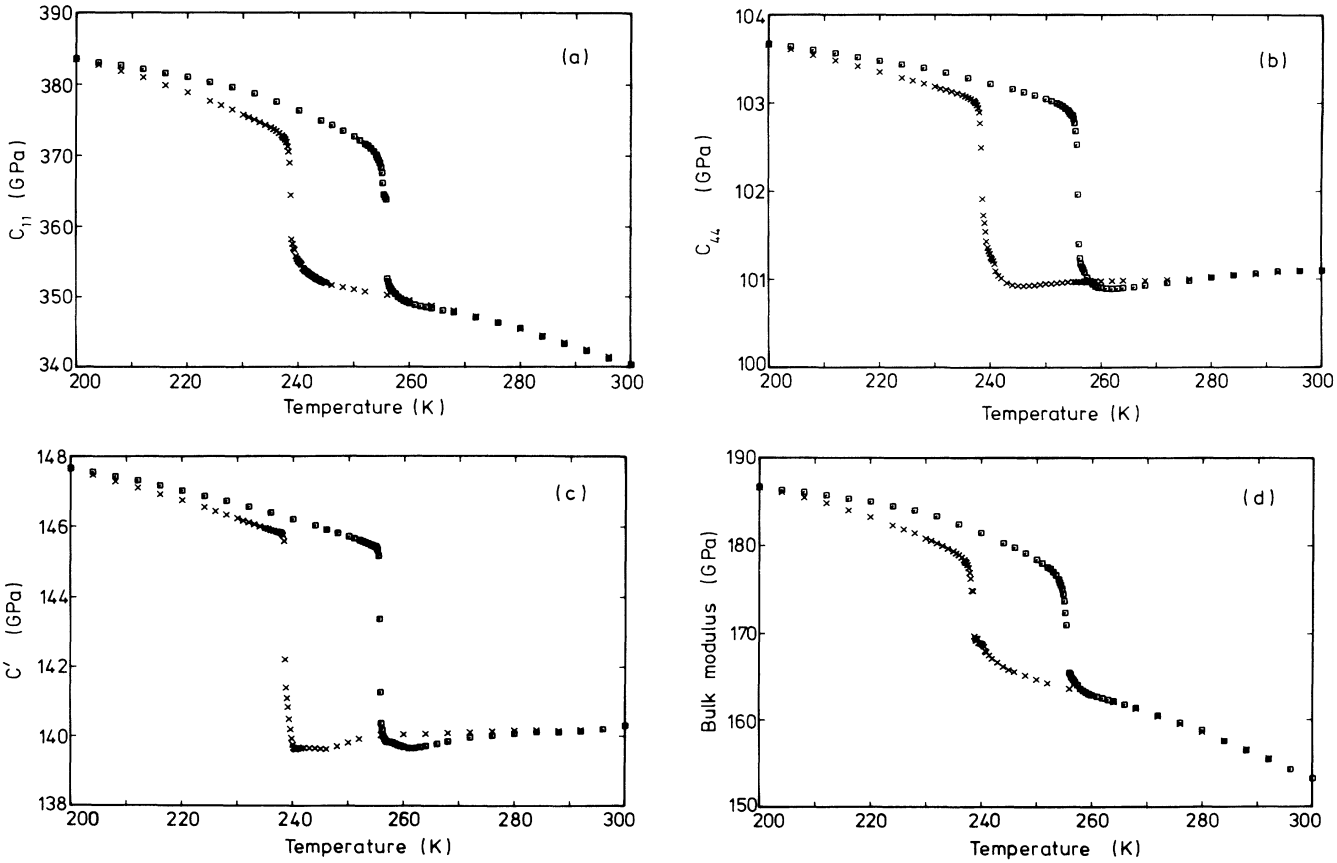

FIG. 1. Temperature dependence of the adiabatic elastic stiffness tensor components (a) C_{11}, (b) C_{44}, (c) C', and (d) bulk modulus B^S of Cr-0.3 at. % Ru. The crosses correspond to ultrasonic wave velocity measurements made with decreasing temperature and the open squares to data as the temperature was increased.

structure, which produces a similar thermal hysteresis in the neutron diffraction data in pure Cr.[2] Because of the pronounced thermal hysteresis of the *I-C* SDW transition, it is essential to state whether experiments are made under conditions of increasing or decreasing temperature. The sharp increase in all elastic moduli at about 238.6 K (during cooling) and the similar drop at about 255.6 K (during warming), together with the hysteresis between about 235 and 257 K, is consistent with the phase transition between the commensurate and incommensurate phase being first order. Hysteresis effects in the temperature dependence of neutron diffraction intensities have also been found near T_{IC} in experiments made[28] on a Cr-0.3 at. % Ru single crystal cut from the same boule as the present sample.

The wave vector Q of the SDW in pure Cr and incommensurate Cr-based alloys is independent of temperature below about 100 K and then increases with temperature.[2,5,67] However, in pure Cr the commensurate phase does not occur: its formation requires donation of electrons to the d band to expand the electron Fermi surface relative to the hole surface. The e/a ratio of Cr-0.3 at. % Ru is 6.006. The *I*-SDW phase is stable at low temperatures;[24] on heating, the wave vector Q of the SDW of this alloy jumps to the commensurate value of $2\pi/a$ at a T_{IC} of 255.6 K. In the case of the dilute Cr-Mn alloys, which have a similar magnetic phase diagram to that of Cr-Ru alloys,[23] the transition from the ISDW phase to the CSDW phase is accompanied by a large expansion of the lattice in the CSDW phase which stabilizes this phase.[29,30] Inspection of thermal expansion results for polycrystalline Cr-0.3 at. % Ru samples[19] shows that the unit cell volume in the CSDW phase is much larger than that in the ISDW phase. Thus it can be inferred that, for the case of Cr-0.3 at. % Ru as well, the anomalous thermal expansion of the lattice at T_{IC} causes the relative shift of the energy bands required to expand the electron jack and contract the hole octahedron: the lattice expands spontaneously to lock in the SDW wave vector Q to the lattice and hence stabilizes the commensurate phase at the expense of the incommensurate phase.

The temperature dependence of the ultrasonic attenuation of the longitudinal and the two shear modes is presented in Fig. 2. The attenuation for each mode is practically independent of temperature in both the CSDW and ISDW phases. The attenuation of the longitudinal C_{11} mode and the shear C' mode is slightly smaller in the low-temperature ISDW phase than in the high-temperature CSDW phase. The *C-I* and *I-C* SDW transitions, which take place on cooling and warming, respectively, are characterized by a sharp attenuation peak (effectively a spike) of only about 0.4 K in width at half amplitude. The position of this attenuation peak, which corresponds to the middle of the steep changes in elastic stiffness moduli (Fig. 1), determine the CSDW-ISDW transition temperature T_{CI} at 238.6 K during cooling, and the ISDW-CSDW transition temperature T_{IC} as 255.6 K during warming.

Outside the transition region the ultrasonic echo trains showed the normal exponential decay. However, in the transition region, the ultrasonic pulse-echo train developed a pronounced interference pattern as the temperature was swept through the transition; the echoes chosen (second and third) to measure the attenuation were sited before the first interference zero. The interference pattern is temperature dependent and its features near the transition temperature are consistent with the coexistence of macroscopic domains of different phases in

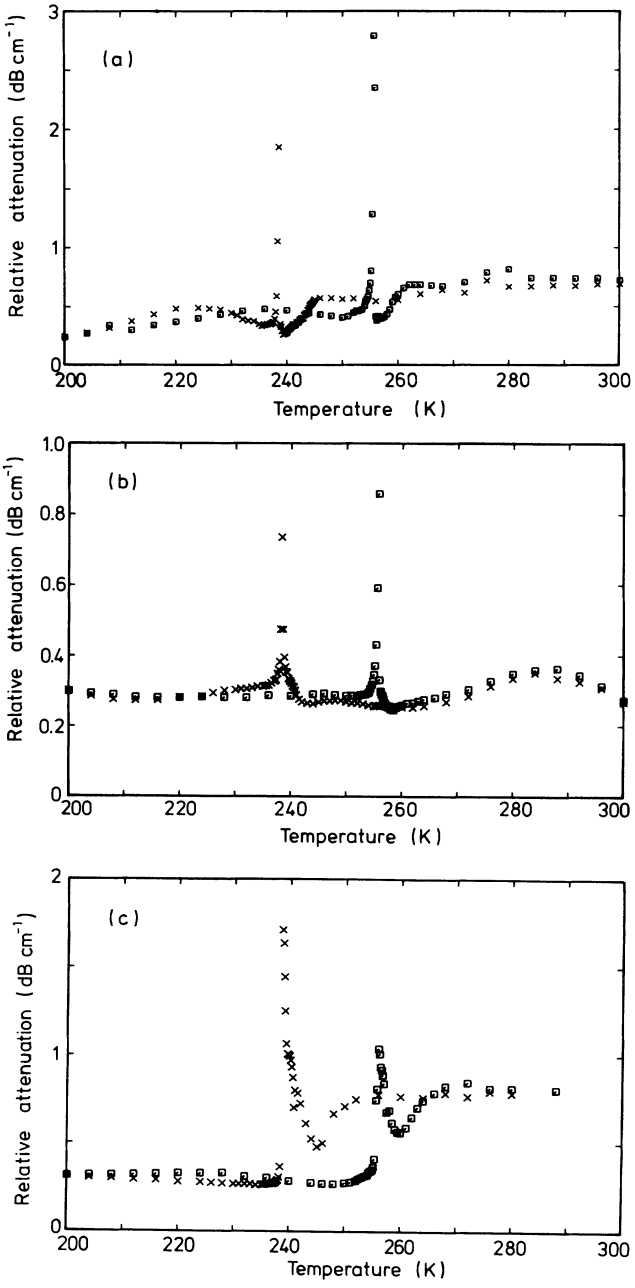

FIG. 2. Temperature dependence of the attenuation of 10-MHz ultrasonic waves: (a) longitudinal mode propagated along the [100] direction, (b) (001) polarized shear mode propagated along the [100] direction, (c) [$1\bar{1}0$] polarized shear mode propaged along the [110] direction in Cr-0.3 at. % Ru. The crosses correspond to measurements made with decreasing temperature and the open squares to data as the temperature was increased.

which the ultrasonic velocity is appreciably different as shown in Fig. 1. These observations provide additional evidence that the commensurate-incommensurate transition is first order. The spike in the attenuation delineates the temperature region where macroscopic domains of the two phases coexist in the sample so that its position can be used to define the transition temperature.

A first-order phase transition in localized antiferromagnets is often accompanied either by a sharp peak or a sharp step in attenuation as a function of temperature.[31] Although in some cases the mechanism responsible for this behavior may be the coupling of ultrasonic waves to low-frequency spin waves, in general it is thought to be due to domains of the two phases coexisting near the transition. Ultrasonic attenuation at the phase transition may result from entropy production associated with the periodic motion of the domain walls due to the different magnetoelastic coupling with the ultrasonic stress in the two phases.

IV. EXPERIMENTAL RESULTS FOR THE HYDROSTATIC PRESSURE DEPENDENCES OF THE ELASTIC STIFFNESS TENSOR COMPONENTS

The results of the measurements of the effects of hydrostatic pressure on the velocities of longitudinal and shear waves propagated along the [100] and [110] directions of Cr-0.3 at. % Ru are presented in Figs. 3–5. These data correspond to the stiffnesses C_{11} (Fig. 3), C_{44} (Fig. 4), and C' (Fig. 5). To show the evolution of the effects of pressure with temperature, the velocity versus pressure data for each mode have been plotted on the same scale at each temperature. The behavior under pressure of the velocities of all modes is most unusual. At room temperature, the velocity of the longitudinal C_{11} mode decreases with increasing pressure: there is pronounced long-wavelength longitudinal-mode acoustic-phonon softening in the commensurate-SDW phase. Both shear mode velocities have a negligible pressure dependence up to about 0.13 GPa. Below room temperature, the pressure dependences of the velocities of each mode are characterized by a steplike increase at a pressure P_{CI} (corresponding to the CSDW-ISDW transition) when the pressure is increased and a similar decrease at P_{IC} (corresponding to the ISDW-CSDW transition) when the pressure is reduced. There is marked hysteresis. Similar results to those found here for the pressure dependence of the velocity of the longitudinal C_{11} mode were observed[21] for the longitudinal mode propagated along the [110] direction which relate to the stiffness C_L $[=(C_{11}+C_{12}+2C_{44})/2]$. These observations also point to strong interactions between the acoustic phonons and the SDW.

With increasing pressure at a given temperature, the crystal transforms from the CSDW to the ISDW phase at P_{CI}. When the pressure is released, the phase transition is reversed with a hysteresis. However, for temperatures below about 258 K, the velocity versus pressure curves

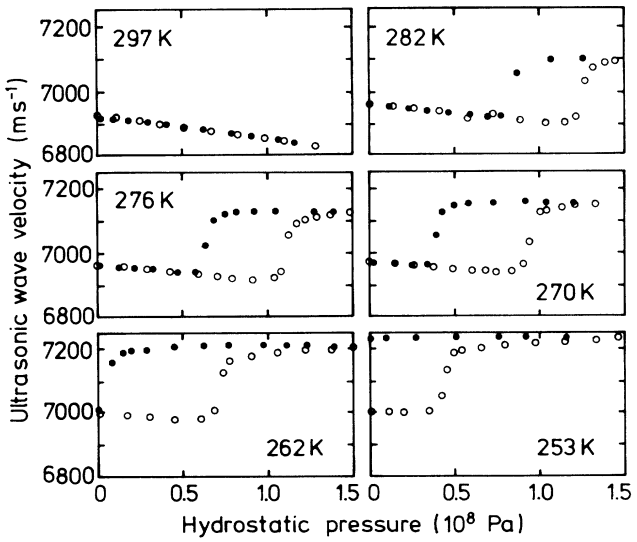

FIG. 3. Hydrostatic pressure dependence of the velocity of longitudinal 10-MHz ultrasonic waves propagated along the [100] direction in Cr-0.3 at. % Ru at the temperatures quoted. The open circles correspond to measurements made with increasing pressure and the filled circles to data as the pressure was decreased.

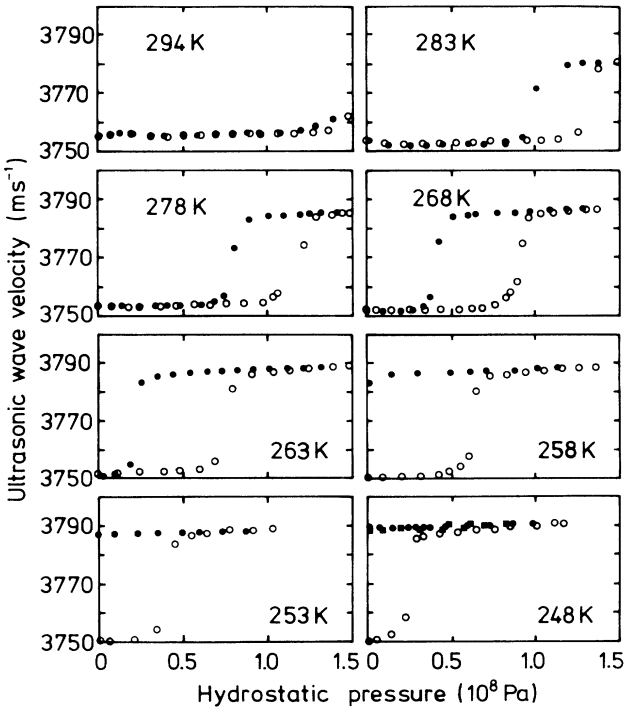

FIG. 4. Hydrostatic pressure dependence of the velocity of shear (001) polarized 10-MHz ultrasonic waves propagated along the [100] direction in Cr-0.3 at. % Ru at the temperatures quoted. The open circles correspond to velocity measurements made with increasing pressure and the filled circles to data as the pressure was decreased. The filled squares in the last panel show the data obtained at 248 K by further pressure cycling after the first cycle and correspond to the frozen-in ISDW phase.

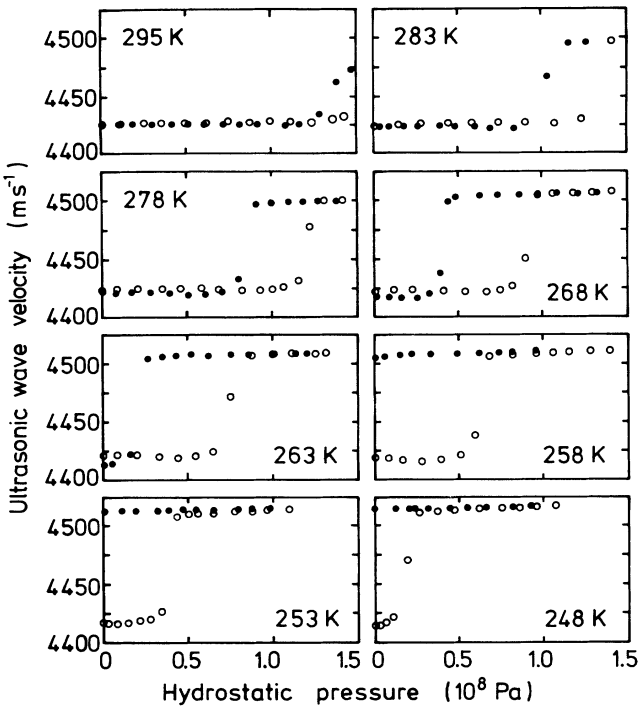

FIG. 5. Hydrostatic pressure dependence of the velocity of $[1\bar{1}0]$ polarized shear 10-MHz ultrasonic waves propagated along the [110] direction in Cr-0.3 at. % Ru at the temperatures quoted. The open circles correspond to velocity measurements made with increasing pressure and the filled circles to data as the pressure was decreased.

for each mode (Figs. 3–5) show that the high-pressure ISDW phase remains frozen in, when the pressure is released. The effect of recycling under pressure on the velocity of the shear C_{44} mode in the frozen-in ISDW phase can be seen in the measurements made at 248 K without allowing the sample to warm up to room temperature (filled squares in the last panel of Fig. 4).

The transition from the CSDW phase to the ISDW phase, which occurs at 238.6 K at zero pressure (see Fig. 1), is shifted up to room temperature (295 K) by applying a hydrostatic pressure of about 0.14 GPa. Therefore the application of pressure on Cr-0.3 at. % Ru produces a similar effect to that induced by a decrease in the e/a ratio, namely, an increase in the temperature range where the incommensurate-SDW phase is stable.

A. The pressure-temperature phase diagram of Cr-0.3 at. % Ru

At the *C-I* and *I-C* SDW transitions, the difference $(V_I - V_C)/V_C$ between the ultrasonic wave velocities in the ISDW and CSDW phase decreases with increasing temperature [Fig. 6(a)]. The normalized velocity change incurred in the ultrasonic wave velocity is approximately the same for the *C-I* and *I-C* transitions and is markedly larger for the longitudinal mode than for the shear modes. The temperature dependence of $(V_I - V_C)/V_C$ for the two shear modes extrapolates to zero at about 315 K. This indicates that the pressure-induced transition from the commensurate to the incommensurate phase will cease at this temperature, and this could be taken as the temperature where the paramagnetic, commensurate-SDW, and incommensurate-SDW phases coexist on the pressure-temperature phase diagram of Cr-0.3 at. % Ru. Support for this suggestion comes from the temperature dependence of the width of the hysteresis $(\Delta P)_T = (P_{CI} - P_{IC})$, which is the difference between the pressures P_{CI} and P_{IC} at which the SDW transition occurs when the pressure is increased or reduced, respectively [Fig. 6(b)]. With increasing temperature $(\Delta P)_T$ decreases, reaching zero at about 315 K. Thus the sharp jump in the ultrasonic wave velocity and the hysteresis effect which characterize the first-order transition from

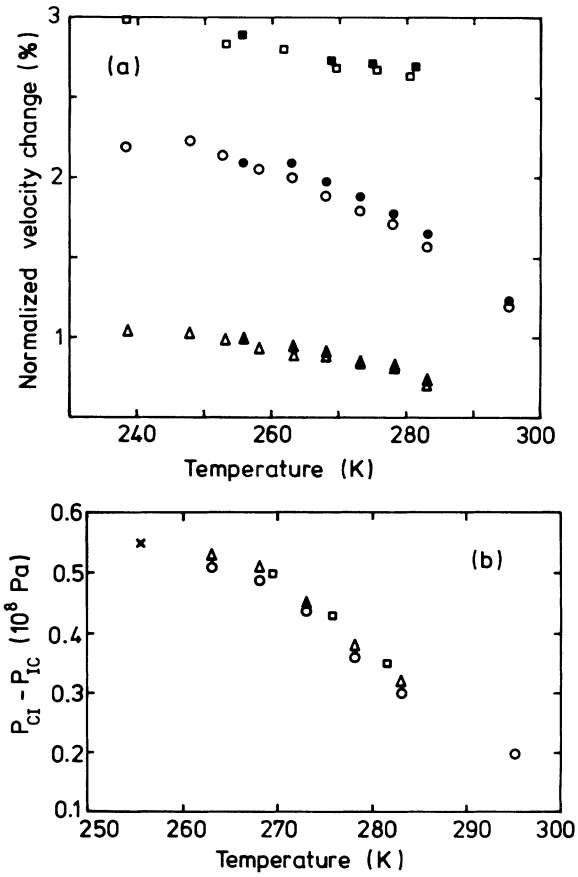

FIG. 6. (a) Temperature dependence of the height $(V_I - V_C)/V_C$ of the sharp step in the ultrasonic wave velocity across the transition obtained from the data given in Figs. 1 and 3–5. The squares correspond to the velocity of the longitudinal mode propagated in the [100] direction, the circles to that of the $[1\bar{1}0]$ polarized shear mode propagated along the [110] direction, and the triangles to that of the (001) polarized shear mode propagated along the [100] direction. The open symbols refer to the *C-I* transition while the filled ones relate to the *I-C* transition. (b) Temperature dependence of the width of the hysteresis. Symbols are the same as in (a). The cross corresponds to all three modes and has been obtained from Fig. 7(a) by taking the pressure difference between the *I-C* and *C-I* lines at T_{IC} (=255.6 K).

the commensurate to the incommensurate phase cease at the same temperature. In the magnetic P-T phase diagram of Cr-0.3 at. % Ru there must be a triple point at about 315 K.

Now the data given in Figs. 3–5 can be used to determine the position of the boundary between the CSDW and ISDW phases on the P-T phase diagram for the cases of both increasing and decreasing pressure. At a given temperature, the pressure P_{CI} where the CSDW-ISDW transition occurs can be taken at the middle of the sharp increase in the velocity versus pressure data obtained with increasing pressure, and likewise the pressure P_{IC}, which corresponds to the ISDW-CSDW transition with decreasing pressure, at the middle of the steep drop in the ultrasonic wave velocity. For Cr-0.3 at. % Ru, both T_{CI} and T_{IC} increase approximately linearly with pressure [Fig. 7(a)]. The mean values of dT_{CI}/dP and dT_{IC}/dP are (333±3) and (277±5) K/GPa respectively, which are comparable with, but more accurate than, those previously quoted in Ref. 21, since the present values have been determined from much larger data sets for more ultrasonic modes. The positive sign of dT_{IC}/dP for Cr-0.3 at. % Ru is the same as that for Cr-Ge (Refs. 32 and 33) and Cr-Mn (Refs. 29 and 34) but it is opposite to that found for Cr-Ga,[35,36] Cr-Fe,[29,34] and Cr-Co (Ref. 34) alloys. The mean value of dT_{IC}/dP for Cr-0.3 at. % Ru is of the same order of magnitude as that found, using other experimental techniques, for all of these dilute Cr alloys.

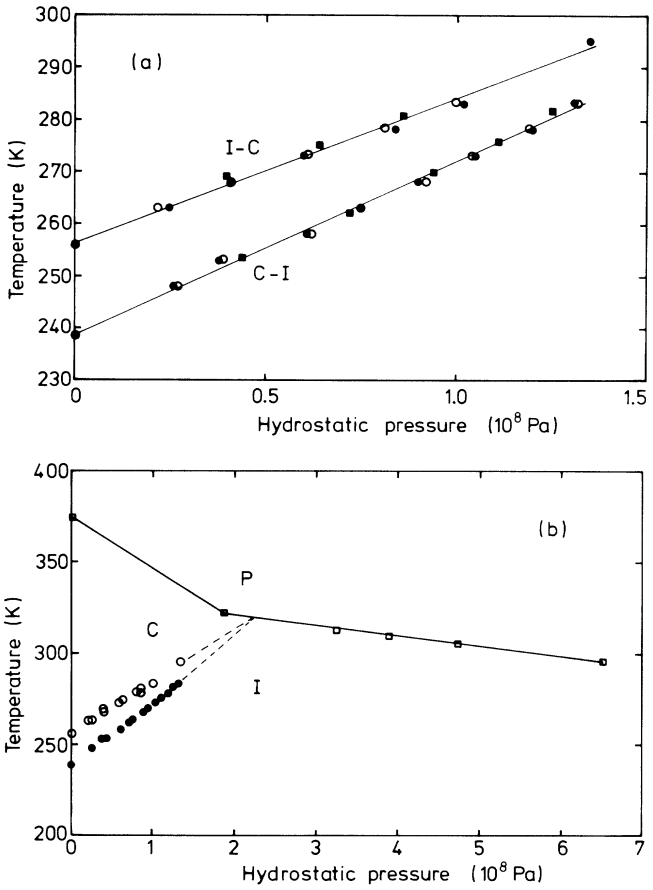

FIG. 7. (a) Pressure dependences of T_{CI} (lower curve) and T_{IC} (upper curve) for Cr-0.3 at. % Ru obtained from the measurements of the effects of hydrostatic pressure on the ultrasonic wave velocities given in Figs. 3–5. The filled squares correspond to the longitudinal C_{11} mode, filled circles to the shear C' mode, and open circles to the shear C_{44} mode. The data at zero pressure are those for all three modes given in Fig. 1. The straight lines are the least-squares fits to the experimental data. (b) The pressure-temperature phase diagram of Cr-0.3 at. % Ru. The open circles (I-C transition, on warming) and filled circles (C-I transition, on cooling) have been obtained from the present ultrasonic data, the open squares and the full lines from Ref. 23. The estimated triple point is at about 315 K and 0.22 GPa.

The pressure-temperature phase diagram of Cr-0.3 at. % Ru is compiled in Fig. 7(b). The boundary between the paramagnetic phase and incommensurate-SDW phase was determined earlier by electrical resistance measurements:[23] this boundary is roughly linear and has a slope of about −50 K/GPa. The phase boundary between the paramagnetic phase and the commensurate-SDW phase had previously been inferred by drawing a straight line from the Néel temperature (377 K) at atmospheric pressure to a point at higher pressure where a sharp change in the slope of the paramagnetic-ISDW phase boundary occurred.[23] However, it had not been possible to determine the I-C boundary, since no anomaly associated with the I-C transition could be detected in resistance measurements. In the present work the phase diagram [Fig. 7(b)] is made more complete by the inclusion of the first-order phase boundary between the commensurate and incommensurate phases with its hysteresis. The magnetic P-T phase diagram of Cr-0.3 at. % Ru alloy has a triple point at about 315 K and 0.22 GPa.

B. Hydrostatic pressure derivatives of the elastic stiffness tensor components

The pressure derivatives $(\partial C_{IJ}/\partial P)_{T,P}$ of the adiabatic second-order elastic stiffness tensor components have been determined from the slope $(\partial f/\partial P)$ of the pressure dependence of the frequency $f(P)$ of round-trips of the ultrasonic pulse in the sample using the relationship[37]

$$\frac{\partial(\rho V^2)}{\partial P}=\rho V^2\left[\frac{2\partial f/\partial P}{f}+\frac{1}{3B}\right], \tag{1}$$

where ρ is the density, V the ultrasonic wave velocity, and B the bulk modulus. The experimental results for the temperature dependences of $(\partial C_{IJ}/\partial P)_{T,P}$ and $(\partial B^S/\partial P)_{T,P}$ for Cr-0.3 at. % Ru in both the incommensurate and commensurate phases are given in Fig. 8. In the incommensurate phase the pressure derivatives of the two shear elastic stiffnesses $(\partial C_{44}/\partial P)_{T,P}$ and $(\partial C'/\partial P)_{T,P}$ are small and positive, while both $(\partial C_{11}/\partial P)_{T,P}$ and $(\partial B^S/\partial P)_{T,P}$ are large and negative [Fig. 8(a)]. Each of these pressure derivatives is only weakly dependent upon temperature in the incommensurate phase. However, their behavior is strikingly different in the commensurate phase [Fig. 8(b)], an exception being $(\partial C_{44}/\partial P)_{T,P}$. In this phase, $(\partial C_{11}/\partial P)_{T,P}$ and $(\partial B^S/\partial P)_{T,P}$ are very large negative quantities and

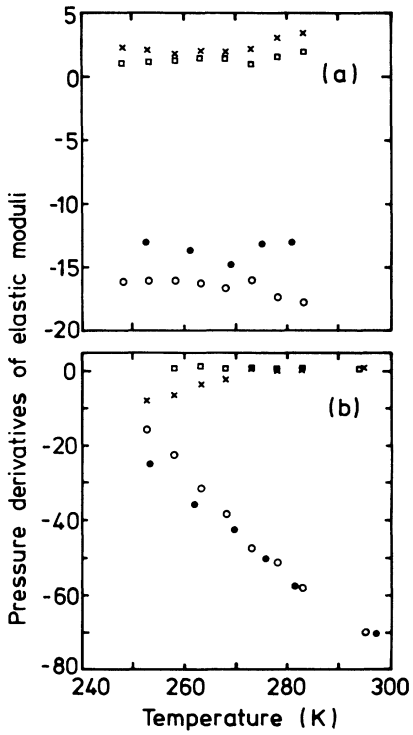

FIG. 8. Temperature dependences of hydrostatic pressure derivatives of elastic stiffnesses of Cr-0.3 at. % Ru (a) in the incommensurate phase and (b) in the commensurate phase: filled circles, $(\partial C_{11}/\partial P)_{T,P}$; open circles, $(\partial B/\partial P)_{T,P}$; squares, $(\partial C_{44}/\partial P)_{T,P}$; crosses, $(\partial C'/\partial P)_{T,P}$.

increase dramatically in magnitude with increasing temperature. The pressure derivative $(\partial C'/\partial P)_{T,P}$ is slightly positive above about 270 K, then goes negative as the temperature is decreased, reaching the large value of -7.8 for a shear modulus at about 253 K [Fig. 8(b)]. In common with its behavior in many magnetic transition metal alloys, $(\partial C_{44}/\partial P)_{T,P}$ has a normal value and shows a weak temperature dependence in both SDW phases: there is little interaction with the SDW for that particular $\mathbf{N}\langle 100\rangle\mathbf{U}\{001\}$ shear mode in contrast to that with the longitudinal modes and the $\mathbf{N}\langle 110\rangle\mathbf{U}\langle 1\bar{1}0\rangle$ shear mode ($\mathbf{N}$ is the propagation direction and $\mathbf{U}$ is the polarization direction).

The application of hydrostatic pressure affects the magnetoelastic coupling between the long-wavelength acoustic phonons and the SDW differently in the commensurate- and incommensurate-SDW phases. In the commensurate phase the behavior of $(\partial C_{11},/\partial P)_{T,P}$ and $(\partial B^S/\partial P)_{T,P}$ with temperature is most unusual: under compression Cr-0.3 at. % Ru becomes easier to squeeze. As a consequence of the magnetovolume effect, there should be a correlation between the hydrostatic pressure derivatives of the elastic stiffness and thermal expansion. Both the thermal expansion and the nonlinear acoustic properties involve the cubic term in the strain energy of the identical irreducible representation η_0^0, which is the volume strain $(\eta_{11}+\eta_{22}+\eta_{33})$. In accord with this there is an anomalous behavior in the thermal expansion: in the commensurate phase, for temperatures about 300 K, the thermal expansion coefficient of polycrystalline Cr-0.3 at. % Ru has a quite small value which decreases with increasing temperature towards T_N and becomes almost zero at about T_N.[19]

As Ru is added to Cr, the stability of the commensurate phase is increased relative to that of the incommensurate phase. Volume expansion can also stabilize the commensurate phase at the expense of the incommensurate phase[30] resulting in a decrease of T_{IC}, that is, $dT_{IC}/dV<0$ which corresponds to $dT_{1C}/dP>0$, as discussed in Sec. IV A. Since the unit cell volume of the commensurate phase is larger than that of the incommensurate phase, the former should be much more sensitive to volume changes induced by application of hydrostatic pressure than the latter. The bulk modulus of the commensurate phase is about 8% smaller than that of the incommensurate phase [Fig. 1(d)]: it is easier to squeeze the material in the commensurate phase where the SDW is locked in to the crystal lattice. This feature is consistent with the unusually large negative values of $(\partial C_{11}/\partial P)_{T,P}$ and $(\partial B^S/\partial P)_{T,P}$.

V. GRÜNEISEN PARAMETERS AND ACOUSTIC-MODE VIBRATIONAL ANHARMONICITY OF Cr-0.3 at. % Ru ALLOY IN THE ISDW AND CSDW PHASES

A negative hydrostatic pressure derivative of an ultrasonic mode velocity, and therefore of the associated elastic stiffness, implies the unusual attribute that under applied stress the long-wavelength acoustic-mode frequency and energy decrease. The dependence of the acoustic-mode frequency ω_p on volume can be expressed as a mode Grüneisen parameter

$$\gamma_p=-\left[\frac{\partial \ln\omega_p}{\partial \ln V}\right]_T, \tag{2}$$

which can be obtained from the measurements of the stiffness tensor components and their dependences on pressure. The acoustic-mode anharmonicity can be quantified by the Grünesisen parameters. For the particular case of volume change induced by an applied hydrostatic pressure, the acoustic-mode Grüneisen parameter γ_p in a phonon branch p of a cubic crystal can be calculated using[38]

$$\gamma_p=-\frac{1}{6w_p}[3B+2w_p+k_p], \tag{3}$$

where

$$w_p=C_{11}k_1+C_{44}k_2+C_{12}k_3$$

and

$$k_p=-k_1\left[C_{11}+3B+3B\left[\frac{\partial C_{11}}{\partial P}\right]_T\right]-k_2\left[C_{44}+3B+3B\left[\frac{\partial C_{44}}{\partial P}\right]_T\right]-k_3\left[C_{12}-3B+3B\left[\frac{\partial C_{12}}{\partial P}\right]_T\right],$$

with

$$k_1 = N_1^2 U_1^2 + N_2^2 U_2^2 + N_3^2 U_3^2 ,$$

$$k_2 = (N_2 U_3 + N_3 U_2)^2 + (N_3 U_1 + N_1 U_3)^2 + (N_1 U_2 + N_2 U_1)^2 ,$$

$$k_3 = 2(N_2 N_3 U_2 U_3 + N_3 N_1 U_3 U_1 + N_1 N_2 U_1 U_2) .$$

Here N_i and U_i $(i=1,2,3)$ are the direction cosines of the wave propagation and the particle displacement directions, respectively. Since the application of pressure can induce the transformation from the CSDW to the ISDW phase at a fixed temperature (Figs. 3–5), it is possible to establish and compare the mode Grüneisen parameters in the two phases at the same temperature. The long-wavelength acoustic-mode Grüneisen parameters γ_p at 278 K, computed for the CSDW and ISDW phases, are plotted as a function of mode propagation direction in Fig. 9. The mode Grüneisen parameters, especially those associated with longitudinal modes, are unusual in both the CSDW and ISDW phases. The longitudinal and quasilongitudinal mode γ_p are negative and much larger in magnitude than those associated with shear and quasishear modes. Furthermore, the longitudinal mode anharmonicity is quite different in the two phases: the absolute values of γ_p for the longitudinal and quasilongitudinal modes in the commensurate phase [Fig. 9(a)] are about four times larger than those in the incommensurate phase [Fig. 9(b)]. The mode γ's in a given branch do not vary substantially with propagation direction.

The acoustic-mode Grüneisen parameters along the fourfold [100] axis are plotted as a function of temperature in Fig. 10. The shear mode $\gamma_S[100]$ has a normal, positive value and is nearly temperature independent in both phases. However, the longitudinal mode $\gamma_L[100]$ is negative in both phases; it is temperature independent in the incommensurate phase [Fig. 10(b)] while its magnitude increases substantially with temperature in the commensurate phase [Fig. 10(a)]. These results are consistent with the behavior of the pressure derivatives of elastic stiffness moduli (Fig. 8), confirming the importance of the interaction between the zone-center longitudinal acoustic phonons and the SDW in the commensurate phase.

The mean long-wavelength acoustic Grüneisen parameter $\bar{\gamma}^{\,el}$ can be calculated by summing all of the long-wavelength acoustic-mode Grüneisen parameters with the same weight for each mode using

$$\bar{\gamma}^{\,el} = \frac{\sum_{p=1}^{3} \int_\Omega \gamma_p \, d\Omega}{3 \int_\Omega d\Omega} . \tag{4}$$

Here the integration is over the whole space Ω. $\bar{\gamma}^{\,el}$ is negative in both phases; its magnitude increases strongly with temperature in the commensurate phase, while it is approximately temperature independent in the incommensurate phase [Fig. 11(a)]. In the incommensurate phase the $\bar{\gamma}^{\,el}$ of Cr-0.3 at. % Ru has a similar magnitude to the thermal Grüneisen parameter γ^{th} $(=1.2)$ for pure Cr.[39]

The variation of $\bar{\gamma}^{\,el}$ with pressure, at a chosen fixed temperature (278 K), is presented in Fig. 11(b). The results obtained for both increasing and decreasing pressure are shown. The most striking feature of the pressure

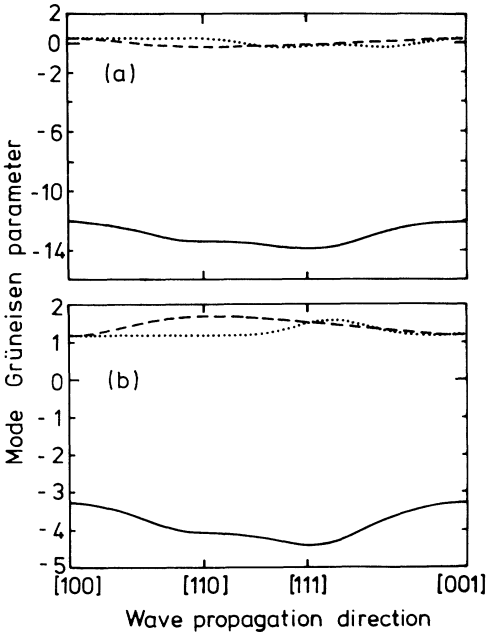

FIG. 9. Long-wavelength longitudinal (solid line) and shear (dashed and dotted lines) acoustic-mode Grüneisen parameters of Cr-0.3 at. % Ru at 278 K as a function of mode propagation direction (a) in the commensurate phase and (b) in the incommensurate phase.

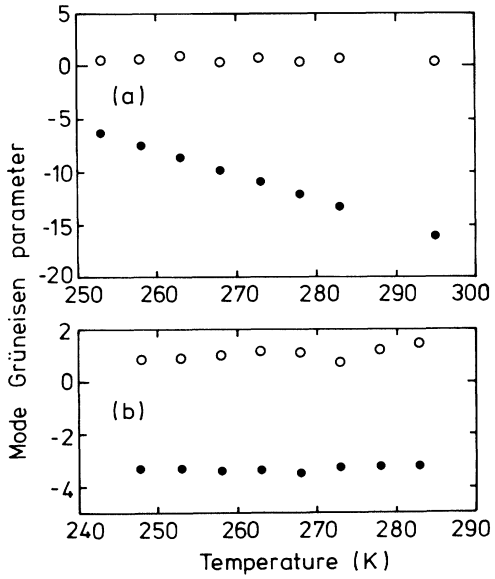

FIG. 10. Long-wavelength longitudinal (filled circles) and shear (open circles) acoustic-mode Grüneisen parameters of Cr-0.3 at. % Ru along the fourfold [100] axis as a function of temperature (a) in the commensurate phase and (b) in the incommensurate phase.

dependence of $\bar{\gamma}^{el}$ is the enormous peak [reaching about 150 at P_{CI} (pressure up) and about 110 at P_{IC} (pressure down)] as the alloy is taken across the phase boundary. This is a consequence of the large change in unit cell volume associated with the first-order character of this phase transition, rather than the sudden change in the mean vibrational anharmonicity of long-wavelength acoustic phonons in Cr-0. 3 at. % Ru in the vicinity of the transition.

The magnetic anomalies observed in the temperature dependence of the thermophysical properties of SDW metals (including Cr and antiferromagnetic Cr alloys) and ferromagnetic $Fe_{65}(Ni_{1-x}Mn_x)_{35}$ Invar alloys have commonly been described in terms of magnetic Grüneisen parameters, which are taken as a measure of the strength of the magnetoelastic coupling.[25,40,41] The magnetic Grüneisen parameter γ_{IC} can be obtained directly from the pressure dependence of T_{IC} using

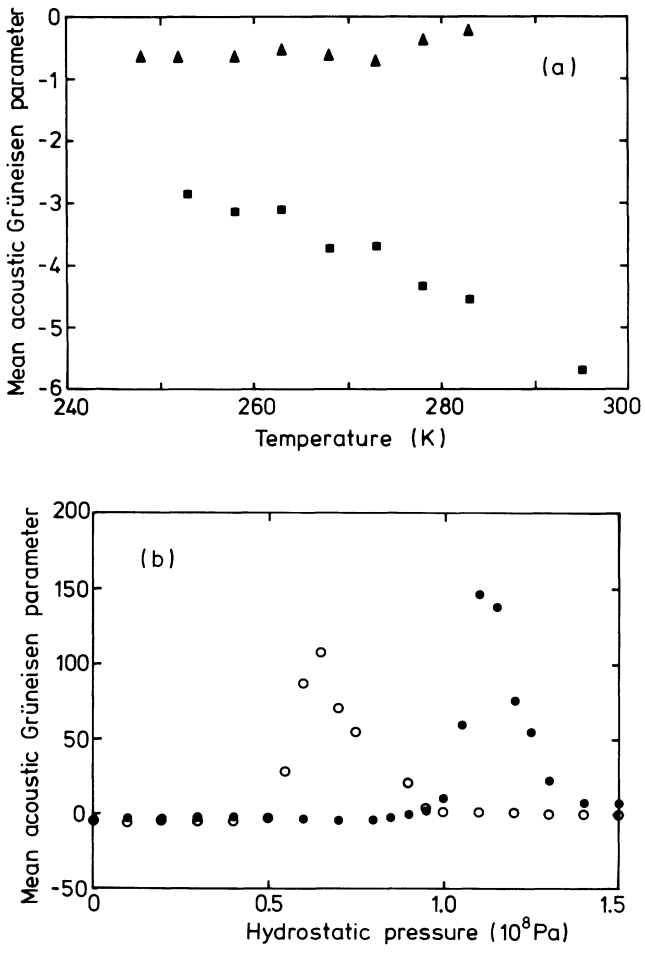

FIG. 11. (a) Temperature dependence of the mean acoustic-mode Grüneisen parameter $\bar{\gamma}^{el}$ of Cr-0.3 at. % Ru in the commensurate (filled squares) and incommensurate (filled triangles) phases. (b) Hydrostatic pressure dependence of $\bar{\gamma}^{el}$ at temperature 278 K: the filled circles correspond to data obtained with increasing pressure and the open circles to data as the pressure was decreased.

$$\gamma_{IC}=B_{IC}\frac{d\ln T_{IC}}{dP}=\frac{B_{IC}}{T_{IC}}\frac{dT_{IC}}{dP}\ , \tag{5}$$

where B_{IC} is the bulk modulus at T_{IC}. Comparison between the bulk moduli of the antiferromagnetic Cr-Ru alloys and that of Cr-5 at. % V alloy, which does not order magnetically, has established that there is a strong magnetoelastic coupling in dilute Cr-Ru alloys both below and above T_{IC}.[19,22,12] From the present data values of 185 and 245 have been obtained for γ_{IC} at T_{IC} and for γ_{CI} at T_{CI}, respectively, which have the same order of magnitude as those determined for other dilute Cr alloys.[12] However, there are fundamental problems associated with assumptions used to develop Eq. (5): the magnetic contribution to the free energy is taken to be separable and to be a function of a single, volume-dependent temperature parameter. In practice it is not possible to separate the magnetic contributions from the electronic or lattice contributions to the free energy.[42–44] In fact the results of the present measurements show that not only the volume strain but also shear strains are involved in the commensurate- to incommensurate-SDW transition. Nevertheless, it is instructive to compare the huge values of the magnetic Grüneisen parameters with the similarly large mean acoustic-mode Grüneisen parameter $\bar{\gamma}^{el}$ in the transition region [Fig. 11(b)].

VI. CONCLUSIONS

(1) Each of the temperature dependences of the velocities of longitudinal and shear ultrasonic waves propagated along the [100] and [110] directions in Cr-0.3 at. % Ru single crystal shows a sharp increase as the alloy is cooled through the commensurate-incommensurate transition temperature T_{CI}. This feature, together with the pronounced thermal hysteresis, establishes that this transition is first order in character. The ultrasonic attenuation exhibits a spikelike peak at the transition.

(2) The adiabatic elastic stiffness tensor components and the bulk modulus are substantially larger in the incommensurate than in the commensurate phase. The relative increases incurred at T_{CI} in the longitudinal C_{11} and the bulk B^S moduli are substantially greater than those in the shear moduli C_{44} and C'. However, while the magnetoelastic coupling is significantly stronger for the volume-dependent longitudinal modes, it also affects the shear modes.

(3) The hydrostatic pressure dependence of the velocity of each ultrasonic mode shows a sharp increase in the elastic stiffness as the alloy is taken through the *C-I* SDW transition and a pronounced hysteresis. The results of these measurements made at fixed temperatures in the range 248–297 K have been used to determine the *C-I* and *I-C* boundaries between the commensurate and incommensurate phases on the *P-T* phase diagram. The magnetic *P-T* phase diagram of Cr-0.3 at. % Ru alloy has a triple point (at about 315 K and 0.22 GPa) where the paramagnetic, commensurate-SDW, and incommensurate-SDW phases coexist.

(4) The incommensurate-commensurate transition temperature increases strongly with pressure; the mean

values of dT_{CI}/dP and dT_{IC}/dP are (333±3) and (277±5) K/GPa, respectively.

(5) The hydrostatic pressure derivatives $(\partial C_{IJ}/\partial P)_{T,P}$ of all independent elastic stiffness tensor components and $(\partial B/\partial P)_{T,P}$ of the bulk modulus have been obtained in both phases as a function of temperature. There is marked longitudinal mode softening in the commensurate and incommensurate phases, that in the former phase being much the larger and strongly temperature dependent.

(6) The experimental results obtained for the pressure dependences of the elastic stiffness moduli on both sides of T_{IC} have established how magnetoelasticity affects the acoustic-mode vibrational anharmonicity in this SDW alloy. The acoustic-mode Grüneisen parameters, which quantify the vibrational anharmonicity in the long-wavelength limit, are negative for longitudinal modes in both phases, having much larger magnitudes in the commensurate phase. The shear mode Grüneisen parameters are small and positive. The strong magnetoelastic coupling at the *I-C* SDW transition takes place mainly with the volume strain, but there are also contributions from shear strain.

(7) The mean long-wavelength acoustic Grüneisen parameter $\bar{\gamma}^{el}$ is negative, being substantially larger and strongly temperature dependent in the incommensurate phase.

(8) There is an enormous peak [reaching about 150 at P_{CI} (pressure up) and about 110 at P_{IC} (pressure down), the same order of magnitude as the magnetic Grüneisen parameter] in the pressure dependence of $\bar{\gamma}^{el}$ as the alloy is taken across the phase boundary. This is attributed to a large change in unit cell volume associated with the first-order character of this phase transition.

(9) The effects of hydrostatic pressure on the elastic behavior of the commensurate phase are much greater than on that of the incommensurate phase: the magnetoelastic interaction between the long-wavelength acoustic modes and the SDW is much stronger in the commensurate phase.

ACKNOWLEDGMENTS

M.C. would like to acknowledge financial support and hospitality of the School of Physics, the University of Bath during his sabbatical visit and a research grant awarded by TÜBITAK (Ankara). H.L.A. would like to thank the South African FRD for financial support.

*Permanent address: Hacettepe University, Department of Physics, Beytepe, 06532 Ankara, Turkey.

[1]A. W. Overhauser, Phys. Rev. **128**, 1437 (1962).
[2]S. A. Werner, A. Arrott, and H. Kendrick, Phys. Rev. **155**, 528 (1967).
[3]E. Fawcett, Rev. Mod. Phys. **60**, 209 (1988).
[4]W. C. Koehler, R. M. Moon, A. L. Trego, and A. R. Mackintosh, Phys. Rev. **151**, 405 (1966).
[5]H. Umebayashi, G. Shirane, B. C. Frazer, and W. B. Daniels, J. Phys. Soc. Jpn. **24**, 368 (1968).
[6]W. J. Venema, R. Griessen, and W. Ruesink, J. Phys. F **10**, 2841 (1980).
[7]W. M. Lomer, Proc. Phys. Soc. London **80**, 489 (1962).
[8]J. Rath and J. Callaway, Phys. Rev. B **8**, 5398 (1973).
[9]D. G. Laurent, J. Callaway, J. L. Fry, and N. E. Brener, Phys. Rev. B **23**, 4977 (1981).
[10]L. M. Falicov and D. R. Penn, Phys. Rev. **158**, 476 (1967).
[11]N. I. Kulikov and V. V.Tugushev, Usp. Fiz. Nauk **144**, 643 (1984) [Sov. Phys. Usp. **27**, 954 (1984)].
[12]E. Fawcett and H. L. Alberts, J. Phys. Condens. Matter **4**, 613 (1992).
[13]D. I. Bolef and J. de Klerk, Phys. Rev. **129**, 1063 (1963).
[14]S. B. Palmer and E. W. Lee, Philos. Mag. **24**, 311 (1971).
[15]K. W. Katahara, M. Nimalendran, M. H. Manghnani, and E. S. Fisher, J. Phys. F **9**, 2167 (1979).
[16]E. E. Lähteenkorva and J. T. Lenkkeri, J. Phys. F **11**, 767 (1981).
[17]W. C. Muir, E. Fawcett, and J. M. Perz, Phys. Rev. Lett. **59**, 335 (1987).
[18]P. C. de Carmargo, E. P. Castro, and E. Fawcett, J. Phys. F **18**, L219 (1988).
[19]H. L. Alberts and J. A. J. Lourens, J. Phys. F **18**, L213 (1988).
[20]H. L. Alberts, J. Phys. Condens. Matter **2**, 9707 (1990).
[21]H. L. Alberts, P. J. Ford, H. Rahdi, and G. A. Saunders, J. Phys. Condens. Matter **4**, 2793 (1992).
[22]H. L. Alberts and A. H. Boshoff, J. Magn. Magn. Mater. **104-107**, 2031 (1992).
[23]A. Jayaraman, T. M. Rice, and E. Bucher, J. Appl. Phys. **41**, 869 (1970).
[24]R. Papoular, D. Debray, and S. Arajs, J. Magn. Magn. Mater. **24**, 106 (1981).
[25]E. Fawcett, A. B. Kaiser, and G. K. White, Phys. Rev. B **34**, 6248 (1986).
[26]E. P. Papadakis, J. Acoust. Soc. Am. **42**, 1045 (1967).
[27]E. Kittinger, Ultrasonics **15**, 30 (1977).
[28]A. H. Boshoff, H. L.Alberts, P. de V. du Plessis, and A. M. Venter (unpublished).
[29]Y. Syono and Y. Ishikawa, Phys. Rev. Lett. **19**, 747 (1967).
[30]B. M. Geerken, R. Griessen, G. Benediktsson, H. U. Aström, and C. van Dijk, J. Phys. F **12**, 1603 (1982).
[31]Y. Shapira, J. Appl. Phys. **42**, 1588 (1971).
[32]J. Mizuki and Y. Endoh, J. Phys. Soc. Jpn. **51**, 3508 (1982).
[33]H. J. van Rijn and H. L. Alberts, J. Phys. Chem. Solids **47**, 937 (1986).
[34]J. Mizuki, Y. Endoh, and Y. Ishikawa, J. Phys. Soc. Jpn. **51**, 3497 (1982).
[35]T. Kaneko, K. Shirakawa, and K. Fukamichi, J. Appl. Phys. **53**, 2459 (1982).
[36]H. L. Alberts and J. A. J. Lourens, Solid State Commun. **50**, 1063 (1984).
[37]R. N. Thurston, Proc. IEEE **53**, 1320 (1965).
[38]K. Brugger and T. C. Fritz, Phys. Rev. **157**, 524 (1967).
[39]G. K. White, R. B. Roberts, and E. Fawcett, J. Phys. F **16**, 449 (1986).
[40]E. Fawcett, Physica B **161**, 83 (1989).
[41]E. Fawcett, M. Acet, M. Shiga, and E. F. Wassermann, Phys. Rev. B **45**, 2180 (1992).
[42]D. J. Kim, Phys. Rev. B **39**, 6844 (1989).
[43]V. L. Moruzzi, Phys. Rev. B **41**, 6939 (1990).
[44]Ll. Mañosa, G. A. Saunders, H. Rahdi, U. Kawald, J. Pelzl, and H. Bach, Phys. Rev. B **45**, 2224 (1992).